In situ study of pentacene interaction with archetypal hybrid contacts: Fluorinated versus alkane thiols on gold

Zhang Jia,* Vincent W. Lee, and Ioannis Kymissis
Columbia Laboratory for Unconventional Electronics, Department of Electrical Engineering, Columbia University, New York, New York 10027, USA

Luca Floreano, Alberto Verdini, and Albano Cossaro
CNR-IOM, Laboratorio Nazionale TASC, Trieste 34127, Italy

Alberto Morgante
CNR-IOM, Laboratorio Nazionale TASC, Trieste, Italy and Department of Physics, Trieste University, Trieste 34127, Italy
(Received 25 June 2010; published 30 September 2010)

One approach developed to improve the performance of bottom contact source/drain electrodes is to treat the contacts with thiols before deposition of the semiconductor. There is evidence indicating that improvement is due to both morphological effects and improved work function matching. Especially suggestive evidence shows that thiols that increase the effective work function of the contacts (e.g., fluorinated thiols) yield better device performance than work function decreasing thiols (e.g., alkane thiols). Here, we compare two technologically relevant thiol treatments, an alkane thiol (1-hexadecanethiol), and a fluorinated thiol (pentafluorobenzenethiol), in pentacene organic field effect transistors. Using *in situ* semiconductor deposition, x-ray photoemission, and x-ray absorption spectroscopy, we are able to directly observe the interaction between the semiconductor and the thiol-treated gold layers. Our spectroscopic analysis suggests that there is not a site-specific chemical reaction between the pentacene and the thiol molecules. A homogeneous standing-up pentacene orientation was observed in both treated substrates, consistent with the morphological improvement expected from thiol treatment in both samples. Our study shows that both the highest occupied molecular orbital–Fermi level offset and C 1*s* binding energy are shifted in the two thiol systems, which can be explained by varied dipole direction within the two thiols, causing a change in surface potential. The additional improvement of the electrical performance in the pentafluorobenzenethiol case is originated by a reduced hole injection barrier that is also associated with an increase in the density of states in the lowest unoccupied molecular orbital.

DOI: 10.1103/PhysRevB.82.125457 PACS number(s): 73.40.−c

I. INTRODUCTION

There has been an intense interest in the surface modification of the source and drain electrodes for organic field effect transistors (OFETs) to improve transistor performance.[1–5] Many printing and lithographic OFET processes pattern the source and drain contacts before the semiconductor is deposited.[6] This bottom contact approach allows processing of the contacts without exposing the semiconductor to process chemicals, which is often detrimental to semiconductor performance. Bottom contact geometries typically have decreased performance when compared with top contact devices, exhibiting both increased contact resistance and reduced channel mobilities. This is due to a morphological mismatch in the semiconductor between the contact and the channel[7] and possibly a barrier to carrier injection at the metal-semiconductor interface.[2,8] A number of thiol-based self-assembled monolayers (SAMs) on the source and drain metal of OFETs have demonstrated improvements to the contact resistance and channel transistor performance.[2,4] Morphological improvement at the contacts, a change in the effective work function of contacts, and charge transfer between the thiols and the semiconductor have been credited with the observed performance improvements.[9]

A number of structural studies have confirmed the ability to engineer the morphology of organic semiconductors deposited on metals via thiol treatment in small molecule[8] and polymer semiconductors.[10] Ultraviolet photoelectron spectroscopy measurements have been performed on a range of SAMs to observe the effective change in the work function[11,12] and led much of the work determining the suitability of these layers to improve organic semiconductor devices.[2,3] In particular, there has been significant work in developing fluorinated thiol treatments for *p*-type organic semiconductors,[5] which effectively increase the work function of the contact layer by creating a dipole layer on the gold. It has been hypothesized that such an interface further decreases the barrier between the semiconductor and the contact, leading to improved access between the contact and highest occupied molecular orbital (HOMO) of the semiconductor. The direct consequent creation of free charge due to the charge withdrawal reaction is also proposed as a reason.[13]

The interaction between thiols and organic semiconductors can be affected by a number of factors including proximity and the final conformation of the material on the surface. The direct observation of surface work function changes caused by a range of thiols on gold has been well studied using photoelectron spectroscopy but *in situ* depos-

ited semiconductor work has primarily focused on the interaction between thiols and gold or organic semiconductors and gold separately. A study of reaction between organic semiconductors and thiol surfaces has attributed the interaction to charge transfer.[13]

Using *in situ* semiconductor deposition together with x-ray photoelectron spectroscopy (XPS) and near-edge x-ray absorption fine structure (NEXAFS), we are able to directly observe the interaction in two technologically relevant organic field effect transistor device stacks. This work directly measures the interaction between pentacene and the two thiols which have been applied to contact improvement in pentacene-based OFETs: an alkane thiol (1-hexadecanethiol) (Ref. 8) and a fluorinated thiol [pentafluorobenzenethiol (PFB)].[14]

II. EXPERIMENT

The two thiol SAMs solutions were prepared with 1% thiol in ethanol. Glass was coated with 5 nm of Cr for adhesion and 50 nm of Au using thermal evaporation. The samples were submerged in the thiol solutions immediately after evaporation to avoid contamination. The experimental samples were mounted on a sample holder with a cold finger for cooling and filaments for heating. Pentacene was evaporated *in situ* in ultrahigh vacuum from a boron nitride Knudsen cell (at ~500 K) while keeping the substrate at room temperature, at a constant rate of 1 Å/min as monitored by a calibrated quartz microbalance. The thickness of single layer (SL) pentacene was calibrated *ex situ* using AFM. In order to prevent radiation damage, we only irradiated the sample with the x-ray beam while the sample temperature was below 210 K. As a check on the integrity of the sample, we periodically monitored the sulfur 2*p* core level, where thiol decomposition on gold would be witnessed by the appearance of a component at a binding energy (BE) 1 eV lower than the characteristic gold-thiolate spectral line at BE=162 eV.[15,16] Thanks to the sample cooling and the spread of the beam over the surface due to the grazing incidence, the thiol structure remained unaltered throughout the measurements.

Measurements were taken at the ALOISA beamline at the Elettra Synchrotron in Trieste, Italy. Core level XPS was measured at photon energy of 450 eV, 650 eV, and 760 eV (photon energy resolution estimated at 150 meV, 250 meV, and 350 meV, respectively) while valence band spectra were taken at 130 eV. Core level photoemission spectra have been aligned against the binding energy of the Au 4*f* peaks.[17] All spectra were taken at a grazing incidence $\alpha=4°$ and close to normal emission ($90°-\alpha$) with an angularly resolved [full width at half maximum (FWHM~3°)] spectrometer. The overall energy resolution for valence band spectra was set to 0.15 eV. NEXAFS spectra were collected at the C *K* edge by means of a channeltron provided with a retarding grid set to −230 V. The x-ray absorption measurements were taken at a constant grazing incidence $\alpha=6°$, in Transverse Magnetic and Transverse Electric polarization (p and s polarization, respectively) by rotating the sample surface around the photon beam axis. Absolute calibration of the photon energy has been obtained *a posteriori* using the fingerprint of carbon contamination in the drain current measured on the gold coating of the last beamline mirror. The corresponding spectral line was previously calibrated by real time acquisition of gas phase x-ray absorption spectroscopy from CO and the drain current.[18]

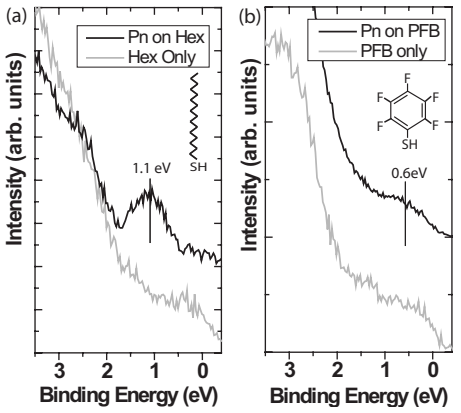

FIG. 1. The valence band edge measured on the (a) hexadecanethiol (Hex-thiol) and (b) pentafluorobenzenethiol (PFB) treated samples. The HOMO edge shifts from 0.5 eV in pentacene/Hex-thiol/Au sample to 0.1 eV in pentacene/PFB/Au sample, showing decreased hole injection barrier from Au contact to pentacene in the latter case which leads to an improved contact between the semiconductor and the source/drain.

III. RESULTS AND DISCUSSION

HOMO states of pentacene deposited on the thiol/Au stack are measured using XPS at a photon energy of 130 eV. Figure 1(a) shows the XPS spectrum for 1-hexadecanethiol (Hex-thiol) on gold (gray line) and the XPS spectrum of a SL of pentacene deposited *in situ* on the 1-hexadecanethiol/gold surface (black line). Likewise, Fig. 1(b) shows the XPS spectra for the (PFB) on gold, both with (black) and without (gray) SL pentacene. For the pentacene deposited on hexadecanethiol [Fig. 1(a)], the HOMO peak is centered at BE =1.1 eV with a FWHM of 0.7 eV. This is consistent with the spectra of SL pentacene grown on silicon dioxide[19] and bulk pentacene (50 nm) grown on gold.[20] The spectrum of the pentacene grown on the pentafluorobenzenethiol [Fig. 1(b)] shows a peak centered at BE=0.6 eV with a FWHM around 0.6 eV. Accordingly, the HOMO edge (as determined by linear extrapolation of the low-binding energy onset) shifts from a binding energy of 0.5 eV in pentacene/Hex-thiol/Au sample to BE≤0.1 eV in pentacene/PFB/Au sample. In the latter case, the decreased hole injection barrier from Au contact to pentacene leads to an improved contact between the semiconductor and the source/drain.

The characteristics of interaction between pentacene and the two thiols can be further analyzed by looking at the respective carbon 1*s* core levels. The C 1*s* XPS spectra, shown in Fig. 2, are taken at a photon energy of 450 eV. The gray lines are from thiols on gold before depositing pentacene and the black lines are the spectra after depositing SL pentacene *in situ*. Again, the spectra are aligned against the bulk com-

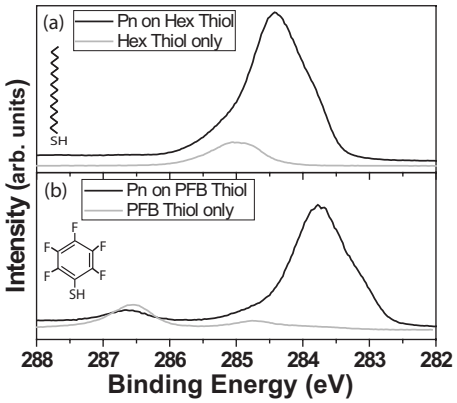

FIG. 2. XPS taken exciting the 1*s* carbon orbital on the (a) hexadecanethiol and (b) pentafluorobenzenethiol samples. The shape of peaks in both samples resembles the shape of peaks in gas-phase and thin-film-phase pentacene formed on nondipole interface. The shift of the C 1*s* peaks in pentacene/PFB/Au to the lower BE is caused by the dipole in the pentacene/PFB/Au.

ponent of the Au 4*f* doublet at 84 eV.[17] The C 1*s* peak for pentacene/Hex-thiol/Au shows an asymmetric shape with two peaks centered at 284.4 eV and 283.8 eV with a FWHM of 0.6 eV and 0.4 eV, respectively. This shape resembles the spectrum of gas-phase pentacene[21] and a monolayer of pentacene on benzenethiol/Cu,[22] which is expected to have same standing-up thin film structure as the pentacene in this experiment. Except for a slight broadening (0.1 eV) and a rigid shift of 0.6 eV to the lower BE for both peaks, the C 1*s* spectrum of pentacene/PFB/Au is the same in shape as that of pentacene/Hex-thiol/Au.

As we later discuss, upon the deposition of a SL pentacene, there may be some charge exchange between pentacene and thiol molecules to align the Fermi energies. However, the similar shape of C 1*s* implies that the electrons withdrawn from or given to pentacene are not preferentially sitting at any of the six nonequivalent carbon atoms in pentacene. We believe the charge exchange occurs only at the shallow HOMO states, where the π electrons are delocalized along the molecule of the pentacene, leaving the core carbon electrons unaffected. Typically, site-specific changes in the core electrons caused by pentacene orientation or changes in the local electronic environment (such as in chemical reaction) appear as either energy or intensity shifts in these two carbon peaks.[22,23] The shape of C 1*s* peaks for pentacene/Hex-thiol/Au and pentacene/PFB-thiol/Au resemble those of thin-film-phase pentacene formed on a nondipolar interface,[23] where there is negligible electronic interaction between pentacene and the thiol surface. As we later indicate, the rigid 0.6 eV shift of the C 1*s* peaks in pentacene/PFB/Au is due to the molecule dipoles with different directions and moments within the two thiols.

Figure 3 showing the C *K*-edge NEXAFS spectra offers verification of the pentacene structure and further evidence of the charge interaction between pentacene and the pentafluorobenzenethiol. For the spectra taken in s-pol, resonance peaks in the lower-energy region (283–288 eV) are assigned to the excitations from C 1*s* core level to the empty π^* orbitals corresponding to the lowest unoccupied molecular orbital (LUMO) (283–285 eV) and LUMO+1 (285–288 eV) transition. The broader features in the high-energy region (292–310 eV) are due to excitations of σ^* orbitals.[18,21,22,24] The resonance peak at 288.8 eV between the above two regions, absent in the gas-phase spectrum,[21] is attributed to molecule-molecule interaction in the deposited pentacene layers.[18,22] Residual contributions from the substrates can be also detected. In particular, the small peak at 287.8 eV in Fig. 3(a) stems from the main transition line of PFB [Fig. 3(d)]. The broader spectrum taken on the HEX substrate additionally affects the LUMO+1 group and the valley at 285 eV between the LUMO and LUMO+1. The intensity difference in π^* region between the s-pol and p-pol absorption spectra indicates the formation of a well-ordered layer of pentacene, with the pentacene molecules preferentially standing up in all samples.[18,22] Similar morphology of pentacene on varied thiols is confirmed by AFM in this study (data not shown) and other studies.[3] This standing-up morphology is important in the operation of pentacene based OFETs.

As a reference, the NEXAFS spectrum of thick (>10 nm) pentacene on a parylene/Au substrate is shown in

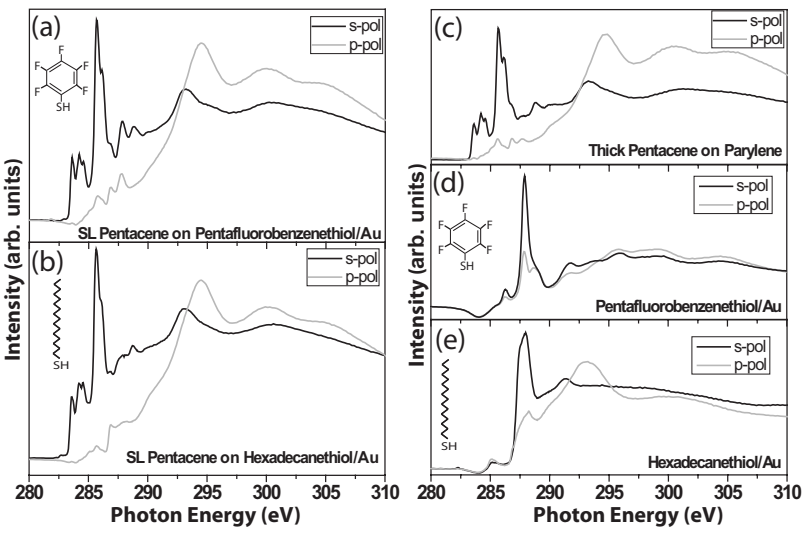

FIG. 3. NEXAFS taken on the (a) pentafluorobenzenethiol with a monolayer of pentacene, (b) hexadecanethiol with a monolayer of pentacene, (c) thick pentacene (>10 nm) on parylene, (d) pentafluorobenzenethiol only on Au, and (e) hexadecanethiol only on Au.

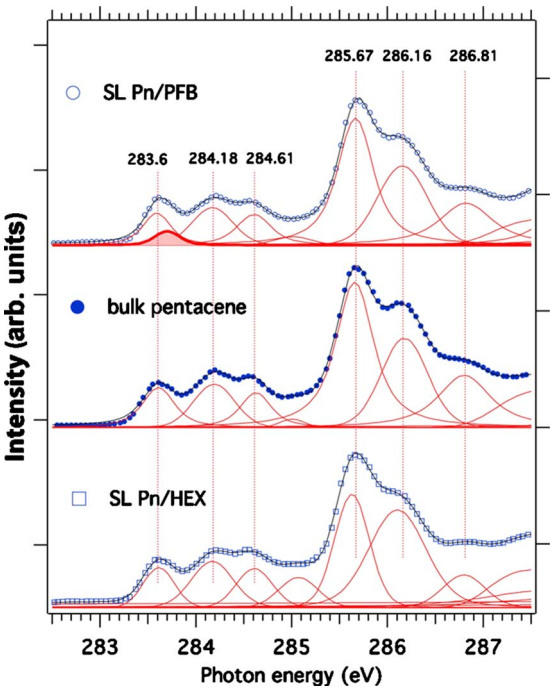

FIG. 4. (Color online) Detailed comparison of the Pn/PFB and PN/HEX LUMO states (open markers in the top and bottom panels, respectively) with the pentacene bulk states from the thick film (filled markers in the middle panel). Multiple component fitting lines are superimposed on the experimental data points. We first fitted the thick film to Voigt functions (full lines) with free-fitting parameters. Then, the NEXAFS spectrum of the Pn/PFB SL was fitted by constraining the LUMO and LUMO+1 states to have the same energy position and shape parameters of the corresponding peaks in the thick film (i.e., only the peak intensity was left as fitting parameter). In the Pn/PFB spectrum, an additional peak (shadowed) accounts for the increase in the density of states at the NEXAFS edge. The fitting constraints were relaxed for the Pn/HEX spectrum in the 285–288 eV range because of the substrate contribution to the NEXAFS spectrum.

Fig. 3(c). The intensity weight of the π^* components for pentacene SL on hexadecanethiol [Fig. 3(b)] and the thick pentacene film [Fig. 3(c)] are comparable to each other. This confirms that there is a negligible charge exchange between the pentacene SL and the hexadecanethiol. However, when pentacene is deposited on the pentafluorobenzenethiol, electron density is transferred from the pentacene band edge (primarily the HOMO shallow states) to the thiol molecules to align the Fermi energies. Electrons then redistribute among the LUMO and HOMO states making available new empty states at the LUMO edge.[25] In Fig. 4, it is clearly seen that the NEXAFS intensity of the first fine structure in the LUMO is enhanced for pentacene grown on pentafluorobenzenethiol. The intensity weight of the first LUMO state also appears larger than in the bulk and than in the gas phase. Because of the atomic-like origin of these fine structures,[21] their relative weight should remain unaltered in the absence of a major rehybridization or of a direct interaction with the substrate of the corresponding atoms. A direct interaction is also excluded since the first LUMO state stems from the six carbon rim-atoms close to the center of the standing-up

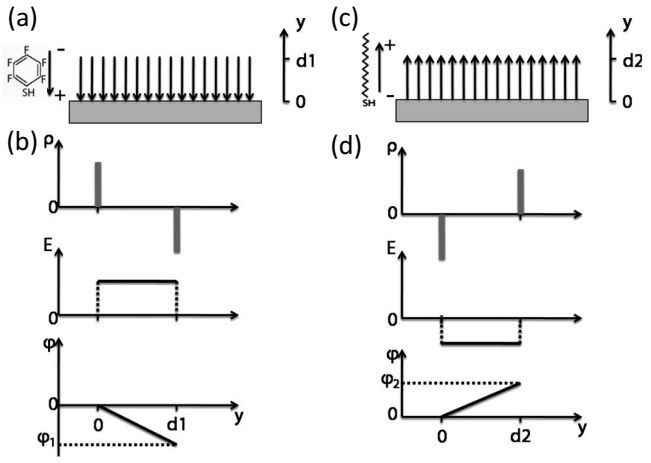

FIG. 5. A schematic of dipole configuration within pentafluorobenzenethiol [(a) dipoles are facing downward to the substrate and hexadecanethiol and (c) dipoles are facing upward from the substrate]. (b) and (d) are the charge, electrical field and potential within the pentafluorobenzenethiol and hexadecanethiol, respectively. The difference of potential on the top of the two thiols ($|\phi_1 - \phi_2|$) with respect to Au is estimated to be 0.4–1.1 eV.

pentacene.[21] The charge retraction from pentacene is effectively pushing a new state above the Fermi level that overlaps the existing LUMO, as evidenced by the LUMO fitting analysis of Fig. 4. For comparison, the reverse mechanism is also observed when injecting electrons into thin organic films by alkali doping; as the LUMO gradually disappears due to charge filling a new state (HOMO) appears below the Fermi level that gradually shifts to lower binding energy as the charge injection increases.[26,27]

When a thiol layer is deposited on Au surface, the surface dipole has two components: the Au-S dipole layer and the dipole layer within the thiol molecules. These dipoles change the surface potential and thus the effective work function of metal.[25] The surface potential shift has the form[28–33]

$$\Delta\phi = N\left(\frac{\mu_{metal^+S^-}}{\epsilon_0} + \frac{\mu_{mol,\perp}}{\epsilon_0\epsilon}\right), \tag{1}$$

where $\Delta\phi$ is the surface potential shift due to a dipole layer, N is the areal density of molecules, $\mu_{metal^+S^-}$ is the dipole moment of the metal-S bond, $\mu_{mol,\perp}$ is the thiol molecule dipole moment projected to the surface normal direction, ϵ_0 is the vacuum permittivity and ϵ is the relative dielectric constant of the thiol molecules. Studies suggest a covalent metal-S bond with a small intrinsic dipole in the self-assembled thiol monolayers on Au and thus the surface potential shift due to the metal-S interaction is small, between +0.02 and −0.05 eV.[33] It is also expected that the $metal^+S^-$ dipole, if any, has the same value for different thiol SAMs.[28] The dipole configuration/direction is shown in Figs. 5(a) and 5(c) for pentafluorobenzenethiol and hexadecanethiol, respectively. The pentafluorobenzenethiol has dipoles facing downward due to the more electronegative F atoms on the top, with normal-axial dipole moment of 1.33D.[34–37] The hexadecanethiol has dipoles facing upward from the surface,[28,33] with the normal-axial dipole moment of 1.5D.[33]

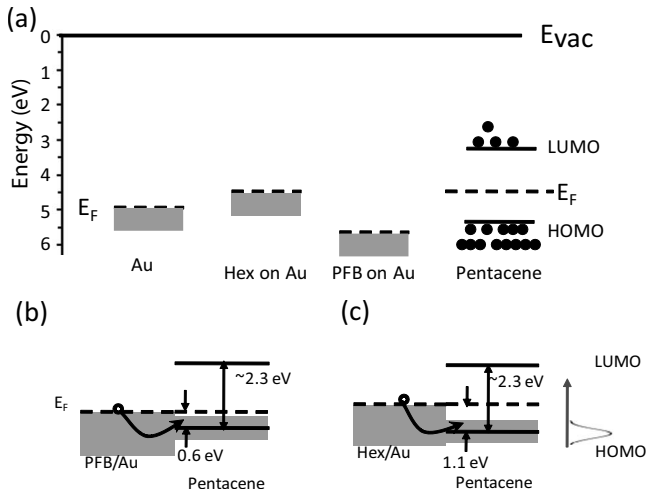

FIG. 6. The energy level model proposed for Au/thiol/pentacene system. In (a), various samples are independently aligned with the vacuum level. Pentafluorobenzenethiol increases the work function of the Au surface while hexadecanethiol slightly decreases the work function of the Au surface. (b) and (c) are bands alignments estimated based on the discussion for pentacene/PFB/Au and pentacene/Hex-thiol/Au samples, respectively, in the text. PFB/Au has improved hole injection barrier as indicated.

Figs. 5(b) and 5(d) are the charge, electrical field and potential with respect to Au underneath within the two thiols, respectively. We assume N is about $1-2\times10^{14}$ cm^{-2} and ϵ is around 2–3. According to the Eq. (1), the surface potential difference ϕ_1-ϕ_2 in the two thiols is about 0.4–1.1 V, consistent with the overall shift of both the C 1*s* core level and valence band for the pentacene deposited on top. The shift of peaks is not present in NEXAFS because the NEXAFS spectra measure the energy difference from C 1*s* states to LUMOs, both of which are equivalently affected by surface potential change.

The band structure of the thiol/pentacene system is shown in Fig. 6. Studies have shown that fluorinated thiols increase the surface work function by 0.5–1 eV while alkane thiols slightly reduce the surface work function by 0.3–0.5 eV.[2,3,11–13] [schematically shown in Fig. 6(a)] The pentacene band structure on the right is from Ref. 32. When pentacene is deposited on the pentafluorobenzenethiol treated Au surface, the Fermi energies align by an electron transfer from pentacene to PFB/Au. This electron transfer is from the weakly bound HOMO state, and does not represent a chemical bond, which would produce inequivalent C atoms. The change in work function of thiol treated Au leads to a different energy alignment with pentacene. The hole injection barrier is $\leq$0.1 eV for pentacene/PFB/Au and ~0.5 eV for pentacene/Hex-thiol/Au, which are derived from HOMO XPS data (Fig. 1). The study of the vacuum level of thiol/Au upon the deposition of pentacene will be valuable to further understand the alignment of vacuum level and such study is underway.

IV. CONCLUSIONS

Electrical measurements of pentacene-based OFETs prepared with thiol treated contacts in the literature have shown improved device performance. By comparing an Alkane thiol (1-hexadecanethiol, Hex-thiol) and a fluorinated (thiol pentafluorobenzenethiol, PFB) layer using *in situ* deposition, XPS, and NEXAFS measurement, we were able to directly observe interactions between the semiconductor and thiol-treated gold layers. HOMO XPS measurement demonstrated a smaller hole injection barrier into pentacene under PFB treatment when compared with Hex-thiol. NEXAFS measurements showed extra available states in the LUMO of the PFB treated device than the Hex-thiol device, indicating that electron density is donated by pentacene to PFB thiol to align their Fermi energies. Core-level XPS measurements and NEXAFS measurements indicated that no site-specific chemical reactions occurs between the thiols and the semiconductor. The NEXAFS measurements also demonstrate a standing-up morphology for both thiol treated samples, which has been demonstrated to lead to superior device performance.[8] We can, on the basis of these measurements, conclude that only morphological improvements lead to improved performance in the case of hexadecanethiol treatments, and both morphological improvements and a reduced charge injection barrier leads to improved performance in the case of pentafluorobenzenethiol treated contacts.

ACKNOWLEDGMENTS

This work was primarily supported by the NSF under Award No. ECCS-0644656, and by the NSEC program of the National Science Foundation under Award No. CHE-0117752 and No. CHE-0641523. The work was also supported through MiUR under Grant No. PRIN2008-prot.20087NX9Y7_002. A.M. gratefully acknowledges the NSEC at Columbia University and the Italian Academy at Columbia University for the warm hospitality and financial support during his visit.

*zj2108@columbia.edu

[1] B. H. Hamadani, D. A. Corley, J. W. Ciszek, J. M. Tour, and D. Natelson, Nano Lett. **6**, 1303 (2006).
[2] J. P. Hong, A. Y. Park, S. Lee, J. Kang, N. Shin, and D. Y. Yoon, Appl. Phys. Lett. **92**, 143311 (2008).
[3] P. Marmont, N. Battaglini, P. Lang, G. Horowitz, J. Hwang, A. Kahn, C. Amato, and P. Calas, Org. Electron. **9**, 419 (2008).
[4] K. Ihm, B. Kim, T. H. Kang, K. J. Kim, M. H. Joo, T. H. Kim, S. S. Yoon, and S. Chung, Appl. Phys. Lett. **89**, 033504 (2006).
[5] C. C. Kuo, Ph.D. thesis, Pennsylvania State University, 2005.
[6] I. Kymissis, A. I. Akinwande, and V. Bulovic, J. Disp. Technol. **1**, 289 (2005).
[7] T. Muck, J. Fritz, and V. Wagner, Appl. Phys. Lett. **86**, 232101 (2005).

[8] I. Kymissis, C. D. Dimitrakopoulos, and S. Purushothaman, IEEE Trans. Electron Devices **48**, 1060 (2001).
[9] D. J. Gundlach, L. L. Jia, and T. N. Jackson, IEEE Electron Device Lett. **22**, 571 (2001).
[10] K. Asadi, F. Gholamrezaie, E. Smits, P. Blom, and B. Boer, J. Mater. Chem. **17**, 1947 (2007).
[11] K. Y. Wu, S. Y. Yu, and Y. T. Tao, Langmuir **25**, 6232 (2009).
[12] C. T. Tseng, Y. H. Cheng, and M. C. M. Lee, Appl. Phys. Lett. **91**, 233510 (2007).
[13] W. Chen, X. Y. Gao, D. C. Qi, S. Chen, Z. K. Chen, and A. T. S. Wee, Adv. Funct. Mater. **17**, 1339 (2007).
[14] J. Smith, R. Hamilton, I. McCulloch, M. Heeney, J. Anthony, D. Bradley, and T. Anthopoulos, Synth. Met. **159**, 2365 (2009).
[15] O. Cavalleri, G. Gonella, S. Terreni, M. Vignolo, P. Pelori, L. Floreano, A. Morgante, M. Canepa, and R. Rolandi, J. Phys.: Condens. Matter **16**, S2477 (2004).
[16] G. Gonella, O. Cavalleri, S. Terreni, D. Cvetko, L. Floreano, A. Morgante, M. Canepa, and R. Rolandi, Surf. Sci. **566-568**, 638 (2004).
[17] A. Cossaro, L. Floreano, A. Verdini, L. Casalis, and A. Morgante, Phys. Rev. Lett. **103**, 119601 (2009).
[18] G. Bavdek, A. Cossaro, D. Cvetko, C. Africh, C. Blasetti, F. Esch, A. Morgante, and L. Floreano, Langmuir **24**, 767 (2008).
[19] N. J. Watkins and Y. Gao, J. Appl. Phys. **94**, 5782 (2003).
[20] P. G. Schroeder, C. B. France, J. B. Park, and B. A. Parkinson, J. Appl. Phys. **91**, 3010 (2002).
[21] M. Alagia, C. Baldacchini, M. G. Betti, F. Bussolotti, V. Carravetta, U. Ekstrom, C. Mariani, and S. Stranges, J. Chem. Phys. **122**, 124305 (2005).
[22] M. Chiodi, L. Gavioli, M. Beccari, V. Di Castro, A. Cossaro, L. Floreano, A. Morgante, A. Kanjilal, C. Mariani, and M. G. Betti, Phys. Rev. B **77**, 115321 (2008).
[23] C. Baldacchini, F. Allegretti, R. Gunnella, and M. G. Betti, Surf. Sci. **601**, 2603 (2007).
[24] S. Söhnchen, S. Lukas, and G. Witte, J. Chem. Phys. **121**, 525 (2004).
[25] H. Ishii, K. Sugiyama, E. Ito, and K. Seki, Adv. Mater. **11**, 605 (1999).
[26] A. Calabrese, A. Floreano, L. Verdini, C. Mariani, and M. Betti, Phys. Rev. B **79**, 115446 (2009).
[27] O. Molodtsova, M. Knupfer, V. Aristov, D. Vyialikh, V. Zhilin, and Y. Ossipyan, J. Appl. Phys. **103**, 053711 (2008).
[28] I. Campbell, S. Rubin, T. Zawodzinski, J. Kress, R. Martin, D. Smith, N. Barashkov, and J. Ferraris, Phys. Rev. B **54**, R14321 (1996).
[29] I. Campbell, J. Kress, R. Martin, D. Smith, N. Barashkov, and J. Ferraris, Appl. Phys. Lett. **71**, 3528 (1997).
[30] S. Howell, D. Kuila, B. Kasibhatla, C. Kubiak, D. Janes, and R. Reifenberger, Langmuir **18**, 5120 (2002).
[31] S. Kobayashi, T. Nishikawa, T. Takenobu, S. Mori, T. Shimoda, T. Mitani, H. Shimotani, N. Yoshimoto, S. Ogawa, and Y. Iwasa, Nature Mater. **3**, 317 (2004).
[32] M. Yoon, C. Kim, A. Facchetti, and T. Marks, J. Am. Chem. Soc. **128**, 12851 (2006).
[33] D. Alloway, M. Hofmann, D. Smith, N. Gruhn, A. Graham, R. Colorado, V. Wysocki, T. Lee, P. Lee, and N. Armstrong, J. Phys. Chem. B **107**, 11690 (2003).
[34] M. Onda and H. Yamada, M. Mori, H. Miyazaki, and I. Yamaguchi, J. Mol. Struct. **319**, 297 (1994).
[35] S. Doraiswamy and S. Sharma, Pramana **2**, 219 (1974).
[36] H. Kang, Y. Kim, M. Hara, and J. Noh, Ultramicroscopy **110**, 666 (2010).
[37] L. Wan, M. Terashima, H. Noda, and M. Osawa, J. Phys. Chem. B **104**, 3563 (2000).